Supplementary information

A gravitationally lensed supernova with an observable two-decade time delay

Supplementary Information For:

A Gravitationally Lensed Supernova with an Observable Two-Decade Time Delay

Steven A. Rodney[1*], Gabriel B. Brammer[2,3*], Justin D. R. Pierel[1],
Johan Richard[4], Sune Toft[2,3],
Kyle F. O'Connor[1], Mohammad Akhshik[5], Katherine E. Whitaker[6,2]

[1]Department of Physics & Astronomy, University of South Carolina,
Columbia, SC 29208, USA

[2]Cosmic Dawn Center (DAWN), Copenhagen, Denmark

[3]Niels Bohr Institute, University of Copenhagen, Jagtvej 128, 2200 Copenhagen N, Denmark

[4]Univ Lyon, Univ Lyon1, Ens de Lyon, CNRS, Centre de Recherche Astrophysique de Lyon
UMR5574, F-69230, Saint-Genis-Laval, France

[5]Department of Physics, University of Connecticut,
Storrs, CT 06269, USA

[6]Department of Astronomy, University of Massachusetts,
Amherst, MA 01003, USA

[*]To whom correspondence should be addressed;
E-mail: srodney@sc.edu, gabriel.brammer@nbi.ku.dk

Telescope	Instrument	Band	UT Date	MJD	Exp. Time [s]
Spitzer	IRAC	3.6 μm	2016-03-15 03:44:04	57462.156	212
Spitzer	IRAC	4.5 μm	2016-03-15 03:44:04	57462.156	241
HST	ACS/WFC	F555W	2016-06-03 21:50:43	57542.910	5214
HST	WFC3/IR	F160W	2016-07-18 23:14:50	57587.969*	1611
HST	WFC3/IR	F105W	2016-07-19 00:43:47	57588.030*	3611
Spitzer	IRAC	3.6 μm	2016-10-13 14:35:13	57674.608	468
Spitzer	IRAC	4.5 μm	2016-10-13 14:35:13	57674.608	581
HST	WFC3/IR	F110W	2019-07-13 20:53:16	58677.870	706
HST	WFC3/IR	F140W	2019-07-14 22:16:01	58678.928	353
HST	WFC3/IR	F125W	2019-07-19 21:27:30	58683.894	706
HST	WFC3/UVIS	F814W	2019-07-21 18:50:53	58685.785	912
HST	WFC3/UVIS	F390W	2019-07-21 19:01:06	58685.792	1272
HST	WFC3/IR	F140W	2019-07-21 22:42:22	58685.946	353
VLT	MUSE	0.4–0.9 μm	2019-09-06 03:56:25	58732.164	2649

Supplementary Table 1: **Record of MACSJ0138 observations used in this work.** Observations in which three images of the SN were detected are marked with an '*' in column five.

Image	Obs. Date (MJD)	Filter	Flux density [μJy]
SN1	57588.03	F105W (Y)	0.18 ± 0.02
SN2	57588.03	F105W (Y)	2.35 ± 0.02
SN3	57588.03	F105W (Y)	0.09 ± 0.02
SN1	57587.97	F160W (H)	1.13 ± 0.04
SN2	57587.97	F160W (H)	3.57 ± 0.05
SN3	57587.97	F160W (H)	0.61 ± 0.04
SN3	58677.87	F110W (Y)	0.01 ± 0.02
SN3	58678.93	F140W (JH)	0.02 ± 0.02
SN3	58683.89	F125W (J)	0.02 ± 0.03

Supplementary Table 2: **Photometry of AT 2016jka.** The final three rows indicate "empty" aperture flux densities measured at the position of image SN3 in the 2019 *HST* visits.

ID	R.A. (deg)	Dec. (deg)	z
H1	24.5099018	-21.9260130	1.95
H2	24.5132090	-21.9299032	1.95
H3	24.5164138	-21.9303172	1.95
H4	24.5176117	-21.9233433	1.95
SN1	24.5151253	-21.9306659	1.95
SN2	24.5123198	-21.9297875	1.95
SN3	24.5100753	-21.9273418	1.95
3.1	24.5169659	-21.9234814	0.7663
3.2	24.5151039	-21.9231406	0.7663
3.3	24.5184361	-21.9264250	0.7663
3.4	24.5146833	-21.9261020	0.7663

Supplementary Table 3: **Multiple images used as constraints in our parametric lens model.** From left to right: image ID, right ascension, declination, spectroscopic redshift. Coordinates are in the J2000 reference frame.

Potential	ΔR.A. [arcsec]	ΔDec. [arcsec]	e	θ [deg]	$r_{\rm core}$ [kpc]	$r_{\rm cut}$ [kpc]	σ [km s^{-1}]
Cluster-DM	$-0.7^{+0.4}_{-0.4}$	$-1.2^{+0.4}_{-0.4}$	$0.81^{+0.02}_{-0.13}$	$114.9^{+2.0}_{-4.1}$	31^{+13}_{-12}	$[1000]$	446^{+52}_{-70}
BCG	$[0.1]$	$[-0.1]$	$[0.52]$	$[-41.1]$	$[0.15]$	136^{+42}_{-32}	700^{+52}_{-57}
P1	$[19.2]$	$[-13.5]$	$[0.49]$	$[86.2]$	$[0.15]$	$[25]$	152^{+30}_{-57}
P2	$[-5.0]$	$[6.9]$	$[0.06]$	$[4.4]$	$[0.15]$	$[12]$	23^{+111}_{-29}
P3	$[-0.8]$	$[-16.7]$	$[0.24]$	$[-63.1]$	$[0.15]$	$[6]$	110^{+35}_{-32}
L* galaxy					$[0.15]$	$[45]$	$[158]$

Supplementary Table 4: **Best fit model parameters for the MACS J0138 mass distribution.** From left to right: mass component, position relative to cluster center (ΔR.A. and ΔDec.), dPIE shape (ellipticity and orientation), velocity dispersion, core and cut radius. The final row is the generic galaxy mass at the characteristic luminosity L*, which is scaled to match each of cluster member galaxies. Parameters in square brackets are fixed *a priori* in the final model (version E).

Method	Data	Lens info	Priors	p(Ia)	p(II)	p(Ib/c)
a. Host color-mag	Host galaxy rest-frame M_K, $B - K$	μ_{host}	-	0.75	0.19	0.06
b. Host stellar pop.	Host galaxy mass & star formation rate	μ_{host}	-	0.62	0.27	0.09
c. SN color-mag	SN F105W-F160W color, m_{F160W}	μ_{SN}	b	0.95	0.01	0.04
d. SN light curve	F105W and F160W SN light curves	μ_{SN}, Δt_{SN}	b	0.94	0.06	<0.01

Supplementary Table 5: **SN classification probabilities for AT 2016jka.** "Lens info" indicates the lensing information used to interpret or derive the observational data: μ_{host} and μ_{SN} are the magnifications of the host galaxy MRG0138 and the SN, respectively; Δt_{SN} refers to the time delays between SN images 1, 2 and 3. In all cases the preferred LENSTOOL model E is used. "Priors" indicates the host galaxy classification probabilities that were adopted as priors for the subsequent classification using SN data.

Supplementary Note: Comparison to Previous Lens Modeling

Ref [1] (hereafter N18) provides a detailed analysis of this cluster, including sophisticated modeling of the lens. The primary modeling in N18 uses a custom lens model code [2] that traces the source Sersic profile(s) through to the image plane and fits the HST images directly. In addition, N18 also made a set of `LENSTOOL` models to estimate the uncertainties. Those models included both source and image plane optimization, and considered both generalized Navarro-Frenk-White (gNFW) [3] and dual pseudo isothermal elliptical (dPIE) density profiles for the cluster. For this work, we used only `LENSTOOL`, only dPIE profiles, and considered only image-plane optimisation because it deals best with actual positional uncertainties. We did not incorporate pixel-level flux data, because the `LENSTOOL` code can only use observed fluxes when doing source plane optimisation (but see further discussion of this in the *Supplementary Note: Host Image Morphology Comparison* below).

Supplementary Table 6 shows the magnification values predicted by our lens model E in comparison to the values reported in N18. Columns 2 and 3 give magnifications for the location of each SN image, while columns 4 and 5 are for the host galaxy images. Column 2 repeats the SN magnifications given in the main text and Supplementary Table 4, which are the expectation values from the μ distributions generated by the `LENSTOOL` MCMC sampling over model parameter space. Column 3 gives the "optimized" SN magnification, which is the μ value returned by the single model instance that has the minimum χ^2 value (note that this may be significantly different from the peak of the μ distribution, as for image 2 in particular). Column 4 reports the minimum-χ^2 magnification at the peak of the surface brightness profile for each galaxy image. Column 5 reports the ratio of the total flux to source flux of the host galaxy, which is effectively a flux-weighted harmonic mean of the magnification factors across each galaxy image. This last value is the most appropriate for comparison to the values of N18 (given in Column 6), which are computed in a similar way. The uncertainties from N18 reflect an estimate of systematic uncertainties, derived from lens modeling variants.

From the last two columns of Supplementary Table 6 we see that our preferred lens model E magnifications are within 1σ of the N18 model, though our predictions are systematically lower by about 20%. This agrees with the assessment of systematic uncertainties from our lens model variants discussed above, which are also shown as the asymmetric error bars on the SN magnitudes in Fig. 2 in the main text, and in Extended Data Fig. 2. As seen in those figures, a larger magnification value would make the SN *more* consistent with the expected luminosity of a Type Ia SN at this redshift— though it would also make it more consistent with some CC SN light curves, likely making the classification somewhat more ambiguous.

It is important to note that the all of the model variants explored here adopted dPIE distributions as the density profile for all lensing components. It is well-documented that the choice of the density profile can strongly affect the inferred magnifications and time delays in a strong lensing system. This

Image	$\langle \mu_{\mathrm{SN}} \rangle$	$\mu_{\mathrm{opt,SN}}$	$\mu_{\mathrm{opt,gal.pk.}}$	$\mu_{\mathrm{gal.avg.}}$	$\mu_{\mathrm{N18,gal.avg.}}$
1	3.9±0.5	6.7	4.35	10.0	12.5±5.4
2	7.4±3	15.2	6.9	8.3	10.3±3.1
3	5±1	4.3	3.64	4.2	4.9±1.6

Supplementary Table 6: **Comparison of magnification predictions with the N18 lens model.**

is therefore another potential source of systematic uncertainty that should be explored in future lens modeling. The models of N18 explored models using gNFW profiles, but of course did not make explicit predictions for the magnifications or time delays at the SN locations. If alternate density profiles result in significant changes to the model-predicted magnfications for the SN images, that could in principle change the conclusions about SN classification and age constraints described here.

We expect that new lens modeling of this cluster with alternate software and different choices of constraints will also be informative, and may improve on our model predictions. Both the N18 modeling and the construction of lens model E and our model variants are constructed blind (without knowledge of the SN magnitudes). Future lens modeling could incorporate the measured magnitudes as constraints, potentially yielding a more robust prediction of the time delay for the fourth image. We hope that the discovery of AT 2016jka will encourage such efforts.

Supplementary Note: Host Image Morphology Comparison

As a qualitative check to evaluate the accuracy of lens model E, we also simulated the overall shape of the SN host galaxy using the sum of two Sersic profiles, and then propagated this through the lens model to make predictions for the morphology of the host arcs. The results are shown in Supplementary Fig. 1 for host images H1-H3 (1.1-1.3). Here we see the model produces a very good match to the observed arcs. This is especially encouraging because the surface brightness distributions of the arcs were not used as inputs for the lens modeling.

The predicted arc morphology for host galaxy image H4 (1.4) is shown in Supplementary Fig. 2. The residuals are more significant, showing clear asymmetric structure, which may indicate a mismatch of rotation and/or shear angle at the location of this image. Nevertheless, the global morphology of the arc is similar in location, size and elongation, which again could be taken as an encouraging indicator of the validity of magnification and time delay estimates for image SN4. For image 5 (not shown), lens model E predicts a very compact source at the location of the BCG, which is at odds with the clearly elongated radial arc of image 5 that can be seen in the HST imaging. This may well be due to the fact that the lens model overestimates the velocity dispersion of the galaxy (see above, and Supplementary Note: Future Lens Modeling). Reconstruction of image H5 is not as important, because the highly demagnified final transient image SN5 is not expected to be observable anyway. Nonetheless, a more accurate reconstruction of host galaxy image H4 (and to a lesser extent image H5), should be an important metric for future lens modeling.

Supplementary Note: Future Work

Future Lens Modeling

The uncertainty in the predicted time delay from the lens model presented here is ± 540 days (in the observer frame). Are there improvements to the lens modeling that could tighten this prediction?

Our lens modeling did not make use of the velocity dispersion of the BCG, measured as 390 ± 10 km s^{-1} from our MUSE data. We did not have this measurement available prior to unblinding, and thus we have restricted ourselves to only consider fully blind lens models in this paper. However, we note that this measured value is very discrepant with the best-fit value of 700 km s^{-1} from our
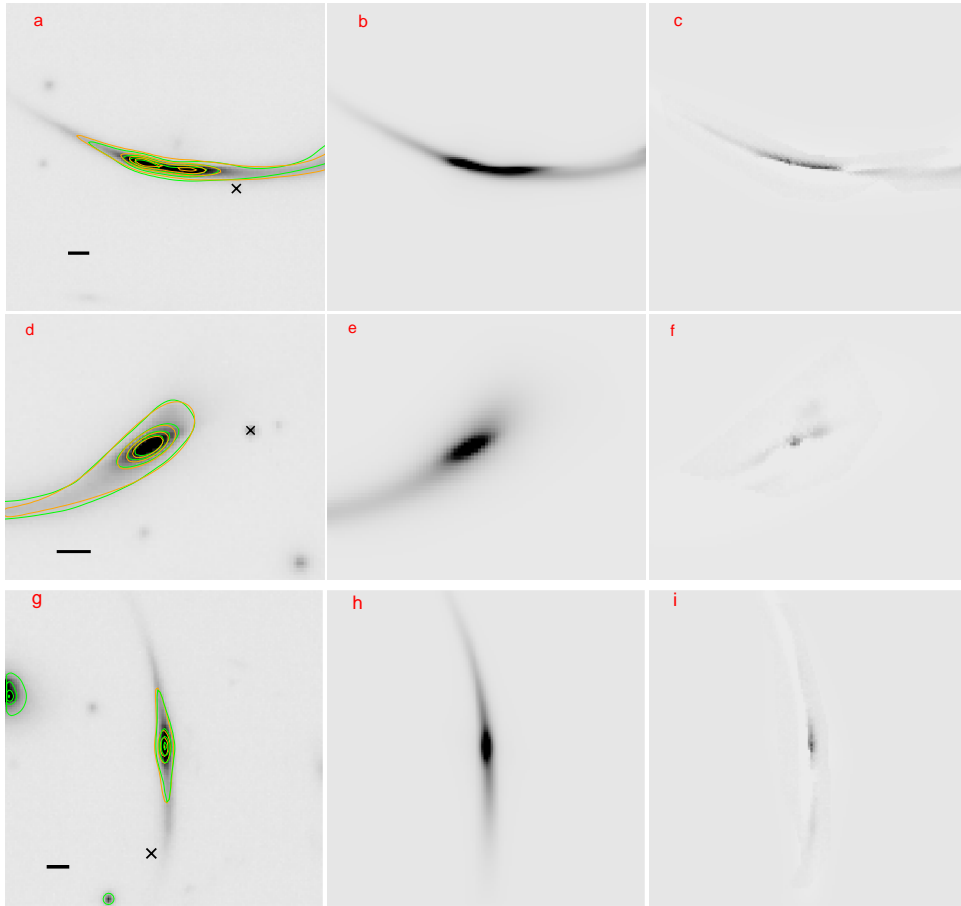
Supplementary Figure 1: **Comparison of the SN host galaxy against a simulation using lens model E.** North is up and East is left. Image 1.1 is shown in the top row, 1.2 in the middle, and 1.3 in the bottom. The left column (panels a,d,g) shows each observed image in the F160W bandpass, with a scale bar indicating 1 arcsecond. The black cross highlights the location of the SN image in each case. The central column (b,e,h) shows a simulated galaxy profile generated using lens model E, with a sum of two Sersic profiles to represent the background galaxy. The last column (c,f,i) shows the residuals (observed-model). Overlaid contours in the first column show the profile of the observed data (green) and the model (orange). The contours are logarithmically spaced and correspond to levels of 1, 2, 4, and 8σ in detection, where σ is the pixel to pixel background level. Some residual flux is apparent in the difference images, but the overall shape of each image is well matched by the simulated profile and the distortions introduced by lens model E.
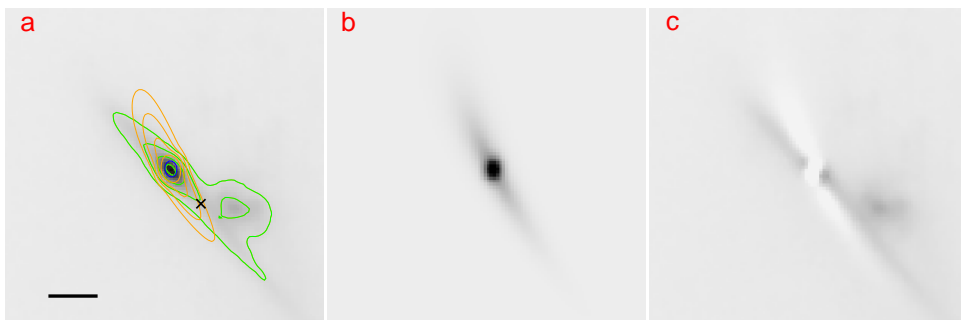
Supplementary Figure 2: **Comparison of the SN host galaxy image 4 against a simulation using lens model E.** Same as Figure 1, but showing galaxy image H4 (1.4).

preferred lens model, variant E (see Supplementary Table 4). Future analyses could incorporate the BCG velocity dispersion and here we speculate about the impact this would have.

With a preliminary extension of model E we find that the time delay predictions would likely shift by <15 days, and the predicted magnifications for SN images 1-3 would likely be larger by as much as ~2.5×. This is within the range of our systematic uncertainty estimates based on lens models A-E. We therefore expect that inclusion of the BCG velocity dispersion will not significantly impact the SN classification or time delay conclusions, but may improve the accuracy and precision of the time delay estimate for image SN4.

One may anticipate that future observations of the lensing cluster (e.g. with JWST) will provide more lens modeling constraints, potentially including the discovery of new multiply-imaged systems and new redshift measurements. These would substantially improve the lens model time delay predictions. Application of different lens modeling approaches could also provide some added confidence that there are not systematic biases in the lens model time delay prediction.

Future Observations

Though the ±540 day time delay uncertainty is small relative to the baseline of > 7000 days, it nevertheless represents a long period over which the field would need to be monitored for the reappearance. Is it feasible to expect future observations to catch the reappearance of AT 2016jka close to peak brightness? Even if the time delay uncertainty remains on the order of ±1 year, it would still be reasonable to execute a follow up campaign with a cadence of approximately 2 months. Since the SN is at a redshift of $z = 1.95$, a span of, say, 50 days in the observer frame is 17 days in the rest frame, comparable to the rise-time of a Type Ia SN. Thus, it is reasonable to expect that a relatively inexpensive monitoring campaign would be able to catch the return appearance of AT 2016jka at or before peak brightness, ensuring a well-sampled light curve for the final SN image.

If future follow-up observations are successful in capturing the full light curve of the final fourth image, then future lens modeling could also incorporate measured SN magnifications as constraints. Measured magnifications from lensed Type Ia SNe have been used to test lens models at both the cluster and galaxy scale [4; 5; 6]. The addition of astrometric constraints for the fourth image could also significantly improve the time delay predictions for a lens model [7]—and this could be done even with a fully blinded analysis. Measurement of the magnification for a lensed Type Ia SN can be done without adopting strong priors from a cosmological model [8], meaning that one can avoid a circular constraint when the AT 2016jka time delay is then used for cosmology.

Future Discoveries

In addition to follow-up observations of AT 2016jka, we may also hope for more discoveries of similar cluster-lensed SNe with long time delays. A primary motivation for pursuing such events is that they can be a relatively low-cost tool for time delay cosmography. As AT 2016jka shows, when the time delay is longer than a few years, the time delay measurement can be anchored at either end by just a few epochs of imaging. If similar events are detected while the SN is still observable, one could collect a well-sampled light curve for an early and bright image using ground-based telescopes. After waiting through the decade-long delay, the SN's reappearance can be captured with a relatively low-cost monitoring campaign. A full light curve of the final image would not be needed. For example,

with AT 2016jka even if the time delay is measured to only ± 150 days, that would be a 2% time-delay measurement, meaning it is lens-model-limited for cosmological inferences.

The expected rate for such events is still highly uncertain, and published rate estimates to date can only be taken as extreme lower limits for the expected yield from future sky surveys [9; 10; 11; 12]. All of these past analyses have been limited to ≤ 5 well-studied galaxy clusters. Furthermore, they have only examined the set of *already known* multiply-imaged galaxies, and have explicitly predicted only the rate of events that would have a time delay of <5 years. With these caveats, the predicted lower limits are of order 1 SN detection per year per cluster, for a deep survey with a detection limit of 27 AB mag [10]. At the 5σ limits of the Rubin Observatory ($i \sim 23.4$ AB mag), the lower limit on that rate is reduced by about a factor of ten [12].

It is treacherous to extend these estimates to the larger population of all galaxy clusters that will be regularly observed by future wide-field surveys. Nevertheless, let us make a crude extrapolation to motivate future work. Consider the 1-year 2000 deg^2 High Latitude Survey (HLS) from the Roman Space Telescope [13; 14], and let us conservatively apply the rate of ~ 1 SN yr^{-1} cluster^{-1} to only the ~ 10 most massive clusters in the HLS area. This still predicts at least 10 cluster-lensed SN detections, which is comparable to the few dozen galaxy-lensed SNe expected from the Roman SN cosmology survey [15]. Similarly, if we apply the $10\times$ lower rate for the Rubin Observatory to the most massive clusters in the LSST survey area, we would anticipate at least ~ 10 detections over the 10-year survey. This discovery rate from wide-field surveys could be enhanced with dedicated ground-based cluster surveys. [16; 17; 9]

We hope that the discovery of AT 2016jka will motivate an improvement over this very rough estimation of future rates. This would require a more complete census of lensing clusters, along with lens models to predict magnifications and time delays, and measurements of star formation and stellar mass in lensed galaxies to predict the SN explosion rates.

References

[1] Newman, A. B., Belli, S., Ellis, R. S. & Patel, S. G. Resolving quiescent galaxies at $z > 2$. II. Direct measures of rotational support. *Astrophys. J.* **862**, 126 (2018).

[2] Newman, A. B., Ellis, R. S. & Treu, T. Luminous and Dark Matter Profiles from Galaxies to Clusters: Bridging the Gap with Group-scale Lenses. *Astrophys. J.* **814**, 26 (2015).

[3] Zhao, H., Analytical models for galactic nuclei. *Mon. Not. R. Astron. Soc.* **278**, 488 (1996)

[4] Nordin, J. *et al.* Lensed Type Ia supernovae as probes of cluster mass models. *Mon. Not. R. Astron. Soc.* **440**, 2742 (2014).

[5] Rodney, S. A. *et al.* Illuminating a dark lens: a Type Ia supernova magnified by the frontier fields galaxy cluster abell 2744. *Astrophys. J.* **811**, 70 (2015).

[6] Dhawan, S. *et al.* Magnification, dust, and time-delay constraints from the first resolved strongly lensed Type Ia supernova iPTF16geu. *Mon. Not. R. Astron. Soc.* **491**, 2639–2654 (2020).

[7] Birrer, S. & Treu, T. Astrometric requirements for strong lensing time-delay cosmography. *Mon. Not. R. Astron. Soc.* **489**, 2097–2103 (2019).

[8] Patel, B. *et al.* Three gravitationally lensed supernovae behind CLASH galaxy clusters. *Astrophys. J.* **786**, 9 (2014).

[9] Riehm, T. *et al.* Near-IR search for lensed supernovae behind galaxy clusters. III. Implications for cluster modeling and cosmology. *Astron. Astrophys.* **536**, A94 (2011).

[10] Li, X., Hjorth, J. & Richard, J. The rates and time-delay distribution of multiply imaged supernovae behind lensing clusters. *J. of Cosmology and Astropart. Phys.* **2012**, 015–015 (2012).

[11] Petrushevska, T. *et al.* Searching for supernovae in the multiply-imaged galaxies behind the gravitational telescope A370. *Astron. Astrophys.* **614**, A103 (2018).

[12] Petrushevska, T. Strongly lensed supernovae in well-studied galaxy clusters with the Vera C. Rubin Observatory. *Symmetry* **12**, 1966 (2020).

[13] Spergel, D. *et al.* Wide-field InfrarRed survey telescope-astrophysics focused telescope assets WFIRST-AFTA 2015 report. *arXiv e-prints* **arXiv:1503.03757** (2015).

[14] Troxel, M. A. *et al.* A synthetic Roman Space Telescope High-Latitude Imaging Survey: simulation suite and the impact of wavefront errors on weak gravitational lensing. *Mon. Not. R. Astron. Soc.* **501**, 2044–2070 (2021).

[15] Pierel, J. D. R. *et al.* Projected Cosmological constraints from strongly lensed supernovae with the Roman Space Telescope. *Astrophys. J.* **908**, 190 (2021).

[16] Stanishev, V. *et al.* Near-IR search for lensed supernovae behind galaxy clusters. I. Observations and transient detection efficiency. **507**, 61–69 (2009).

[17] Goobar, A. *et al.* Near-IR search for lensed supernovae behind galaxy clusters. II. First detection and future prospects. *Astron. Astrophys.* **507**, 71–83 (2009).